Journal of Materials Chemistry C

PAPER

View Article Online
View Journal

Cite this: DOI: 10.1039/c7tc02926h

A flexible and highly sensitive capacitive pressure sensor based on conductive fibers with a microporous dielectric for wearable electronics†

Ashok Chhetry, Hyosang Yoon and Jae Yeong Park *

In this study, a flexible and highly sensitive capacitive pressure sensor has been fabricated by coating a microporous polydimethylsiloxane (PDMS) elastomeric dielectric onto conductive fibers. Conductive fibers were prepared by depositing silver nanoparticles (AgNPs) in poly(styrene-*block*-butadiene-styrene) (SBS) polymer on the surface of Twaron fibers. The configuration obtained by cross-stacking of two microporous PDMS-coated fibers imitates a capacitive sensor, which responds to compressive stress by increasing the contact area and decreasing the separation between the fiber electrodes. Moreover, the gradual closure of micropores under pressure increases the effective permittivity of the dielectric, thereby enhancing the sensitivity of the sensor. A relatively high sensitivity of 0.278 kPa^{-1} for a low pressure region (<2 kPa), negligible hysteresis of 6.3%, a dynamic response time in the millisecond range (~340 ms), a low detection limit of 38.82 Pa and an excellent repeatability of over 10 000 cycles were achieved. Finally, the practicality of the sensor was also demonstrated by loading small objects (~9.4 mg) and gentle finger touches (<10 kPa). By virtue of its excellent sensitivity, low pressure detection and cost-effective fabrication process, our sensor is applicable for next-generation advanced touch panels with a more human-friendly interface, non-invasive health monitoring systems, and artificial robot arms.

Received 29th June 2017,
Accepted 13th September 2017

DOI: 10.1039/c7tc02926h

rsc.li/materials-c

Introduction

The development of highly sensitive wearable pressure sensors that are inexpensive and easy to manufacture has attracted extensive interest in the measurement of physical signals generated by the human body. Promising routes towards the development of new sensing materials, fabrication processes and sensing mechanisms have contributed to significant progress for the implementation of flexible and stretchable physical sensing devices. These physical sensors enable various applications such as electronic-skin (e-skin),[1–3] human–machine interfaces,[4–7] health-status monitoring,[8–11] human-activity monitoring,[12] proximity sensing,[13] and others. For simple and low cost preparation of flexible and wearable electronics, fibrous materials have become attractive for use due to their high electrical conductivity and mechanical endurance against external deformation.[14,15] Various transduction principles such as capacitive,[5,16–19] piezoresistive,[4,6,20,21] piezoelectric,[8,22,23] and optical[24,25] have been intensively investigated to ensure unique superiority such as high performance, low-modulus, light-weight and conformal contact to the human body. In particular, capacitive type sensors are viewed as a preferable type for high sensitivity, low power consumption, simple fabrication process and better immunity to temperature.[26,27]

For the fabrication of conductive textiles, various materials such as conductive polymers, carbon based materials and metallic materials have been explored in the literature.[14,28,29] The electrical properties of such conductive fibers fabricated from various materials are compared in Table 1 along with their merits and demerits. Metallic material based conductive fibres are widely preferred for simple, low cost, highly conductive and stable requirements. Such conductive fibers have been fabricated by different methods such as electroless deposition,[32,33] dip-coating,[29,34] wet spinning,[35,36] and chemical solution processes.[14] Electroless deposition of metals on polymer fibers is not suitable for stretchable electronics since the fiber cannot retain good electrical properties under strain.[37] Conductive polymers, on the other hand, have a crucial role in energy storage devices, supercapacitors, fuel cells, *etc.* but the limitation is that the electro-chemical stability of the polymer coated conductive fibrous material decays with time. In recent years, various metallic nanomaterials mixed with polymers have regained much interest mainly due to their high electrical conductivity, stability against oxidation and antimicrobial activity.[5,14,36]

Department of Electronic Engineering, Kwangwoon University, 447-1 Wolgye-dong, Nowon-gu, Seoul 01897, Korea. E-mail: jaepark@kw.ac.kr

† Electronic supplementary information (ESI) available. See DOI: 10.1039/c7tc02926h

Table 1 Characteristics of the conducting fiber materials and their electrical properties

Types	Materials	Advantages	Disadvantages	Electrical property	Ref.
Conductive polymer	PEDOT:PSS	Simple growth technique	Slow coating of polymer	50–60 Ω cm^{-1}	28
Carbon materials	Graphene	Easy to attach material film	Multiple steps, complex process	10–20 S cm^{-1}	30
Metal based materials	Aluminum	Low cost	Needs catalyst for decomposition	0.2 Ω cm^{-1}	13
	Ag nanowires	Stretchability	Surface modification	0.8 Ω cm^{-1}	31
	Ag nanoparticles	Highly conductive	Optimization required	0.1431 Ω cm^{-1}	This work

For the dielectric structures of the capacitive sensors, various microstructured materials have been employed to improve the sensing capability as well as short response times. Two-dimensional pyramid-shaped microstructure arrays,[17,38–40] domes,[41] and micro-pillar arrays[42] have also been reported in the literature. However, the fabrication of such structures requires a microstructured silicon mold that makes the fabrication process quite expensive.

In this work, we report a facile and cost effective approach to fabricate a flexible and highly sensitive capacitive pressure sensor based on conductive fibers. The coating of a microporous dielectric thin film on the surface of conductive fibers was achieved for the first time in the literature. The strategy of micro-structuring the dielectric material is to leverage the sensor's performance by enhancing the effective permittivity and reducing the stiffness. Our approach enables a simultaneous change in the structural behavior of three major parameters of the capacitor. Therefore, the capacitance response of the sensor significantly increased with applied pressure not only as a result of increased effective permittivity, but also as a result of reduced distance between electrodes and increased area of the electrodes. The conductive fibers were obtained by coating SBS polymer on the surface of Twaron fibers with absorption of silver trifluoroacetate ($AgCF_3COO$) followed by reduction of an Ag precursor into AgNPs by hydrazine hydrate ($N_2H_4{\cdot}4H_2O$). Twaron fibers were chosen as a substrate material for the conductive fibers due to their properties such as high dimensional stability, excellent strength-to-weight ratio, and resistance to heat, flames and chemicals. For the dielectric material, PDMS was chosen because of its high chemical and thermal stability, low elastic modulus, and eco-friendliness. Glucose particles were used as the pore creating fillers. The sensor with a microporous dielectric possessed an excellent sensitivity of 0.278 kPa^{-1} for <2 kPa, a short response time in the millisecond range, and a wide dynamic range from 0–50 kPa along with an excellent repeatability of over 10 000 cycles. In addition, the approach that we developed efficiently exploits features such as flexibility and stretchability.

Experimental

Fabrication of conductive fibers

Fig. 1a represents a schematic illustration of the overall process for the fabrication of a fiber-based capacitive pressure sensor. The fabrication of the conductive fibers involves three main steps: (i) SBS coating onto the surface of Twaron fibers, (ii) absorption of an Ag precursor into the SBS polymer layer, and (iii) reduction of the Ag precursor into AgNPs. Twaron fibers of diameter ~230 μm were cut into 16 cm lengths and vertically laid on the substrate by suspending a 150 g weight.

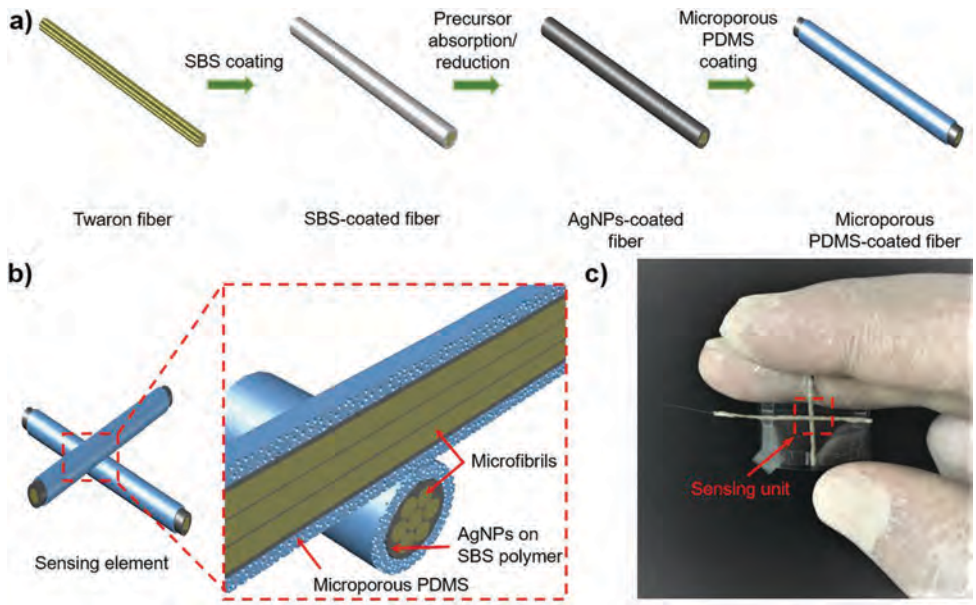

Fig. 1 (a) Schematic process for the fabrication of a fiber-based capacitive type pressure sensor. (b) Schematic of the cross-sectional view of the sensing unit. (c) Photographic image of the sensor fabricated on PET sheets.

A SBS polymer (5 wt%) dissolved in a mixed solvent of tetrahydrofuran and dimethylformamide (3 : 1 weight ratio) was coated along the vertical fibers by flowing 4 mL of solution at a flow rate of 2 mL s^{-1}. After 5 minutes of evaporation in air, the SBS coated fibers were immersed in a solution of $AgCF_3COO$ (15 wt%) and ethanol for 30 min. To generate the AgNPs on the SBS layer, the absorbed Ag precursor was reduced by a solution of $N_2H_4{\cdot}4H_2O$ (20–26% in water) in ethanol and deionized water (1 : 1 volume ratio).

Fabrication of the microporous elastomer and sensors

Glucose particles purchased from a market were lightly ground to make them smaller and uniform in size, washed with hexane and then magnetically stirred for 2 h until hexane evaporated. A mixture of PDMS base and curing agent (10 : 1 weight ratio) with glucose particles was ultra-sonicated for 30 min and mechanically stirred for another 30 min for uniform mixing. Then, the suspension was coated on the surface of the conductive fibers in the same way as used for coating of the SBS polymer. After curing of the microporous PDMS-coated fibers in a convection oven at 72 °C for 3 h, one cross-sectional side was trimmed away by a razor blade, and then dipped into deionized water for 48 h to dissolve the glucose particles. After that, such fibers were washed under sonication for 5 h, and finally, dried at 60 °C for 3 h to get a porous structure. A capacitive type fiber-based pressure sensor was formed by stacking two such microporous PDMS-coated fibers perpendicular to each other. Fig. 1b illustrates a schematic of the orthogonally stacked fibers and the inset illustrates the cross-sectional view of the sensing unit. Fig. 1c provides a photographic image of the sensor fabricated on a flexible poly(ethylene terephthalate) (PET) sheet. For comparison of the sensor characteristics, a reference sensor was also fabricated by coating a solid PDMS dielectric on the conductive fibers. Both fabrications were carried out on conductive fibers of the same electrical and mechanical properties under the same environment.

Characterization and measurements

The surface morphology of the conductive fibers and pore structure of microporous PDMS were examined using field emission scanning electron microscopy (FE-SEM) and X-ray microcomputed tomography (micro-CT). Electrical linear resistance (ELR) was measured using an Electrometer (Keithley 6514). To apply a precise load, a moving stage (JSV-H1000, Japan Instrumentation System Co., Ltd) in combination with a force gauge (HF-1, Japan Instrumentation system Co., Ltd) along with an Acrylic spacer (2 mm × 2 mm × 1 mm) in between the sensor surface and force gauge fixture were used. The use of the spacer offers improved lamination between the sensor and force gauge tip, and also provides uniform force over the sensor enabling measurement of very low pressures.[17] The T-speed of the force gauge was set to 1 mm per minute with a stroke of 1.3 mm. Capacitance measurements were performed using an LCR meter (Hioki IM 3536) at 100 kHz frequency with a 1 V AC signal. A computer was employed to record the compression distances, forces and capacitances. A digital oscilloscope (TDS5052B Digital Phosphor Oscilloscope, Tektronix) was also used for the measurement of the signal at the output of the capacitance readout circuit.

Results and discussion

Theoretical consideration

The schematic illustration in Fig. 2a represents the cross-sectional view of the sensing unit and Fig. 2b represents the structural change in behavior under the application of an external pressure. The capacitance generated at the cross point of two fibers is effectively changed by applying incremental forces, which induces deformation in the thickness. When external pressure is applied, the distance between the electrode fibers is reduced (from d to d'), the contact area between the electrodes is increased (from A to A'), and most importantly, the effective permittivity of the dielectric material is increased (from ε_r to ε_r'). Specifically, the permittivity of the dielectric material is calculated by,

$$\varepsilon = \varepsilon_o \varepsilon_r,$$

where $\varepsilon_o = 8.854 \times 10^{-12}$ F m^{-1} is the free space permittivity and ε is the relative permittivity of the dielectric material. For the microporous dielectric layer, an effective relative permittivity is the combined effect of PDMS ($\varepsilon_p \approx 3$) and air ($\varepsilon_a \approx 1$) inside the micropores, which is estimated by $\varepsilon = \varepsilon_a f + (1 - f)\varepsilon_p$. Where ε_a and ε_p refer to the permittivity of air and solid PDMS, respectively. The parameter f relates to the vacuum fraction in the microstructured PDMS. When an external pressure is applied to the sensor, the vacuum fraction which has lower permittivity is reduced due to the closure of the micropores resulting in increased effective permittivity since the micropores are replaced by surrounding PDMS. The theoretical analysis of the dependency of the rate of capacitance change with the rate of permittivity change and elastic modulus due to inclusion of micropores is provided in the ESI.†

A stable and uniform thin film (~70–90 nm) of SBS polymer was coated on the surface of Twaron fiber. The film can stay uniform along the fiber by saturating the Rayleigh–Plateau instability provided the film thickness satisfies[43]

$$h < \rho g R^3/\gamma,$$

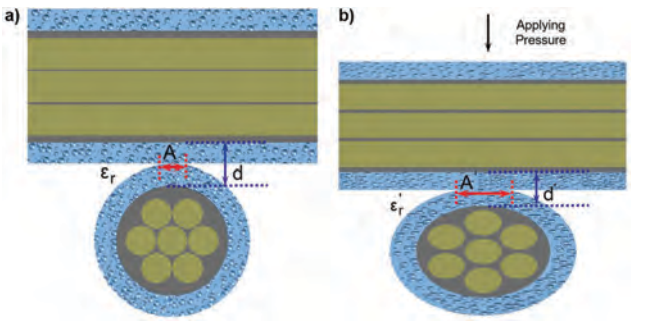

Fig. 2 (a) Schematic of the cross-sectional view of the sensing unit. (b) Schematic illustration showing the structural change in behavior of the sensing unit under an external pressure.

where h is the film thickness, ρ is the density of the polymer, g is the acceleration due to gravity, R is the radius of the coating fiber, and γ is the surface tension of the polymer. A stable and continuous film flowing down a vertical fiber is obtained for sufficiently low flow rates. Thanks to the advection of the flows. When SBS coated fibers are immersed into solutions of $AgCF_3COO$, trifluoroacetate anions (CF_3COO–) form ion–dipole interactions with the hydroxyl groups (–OH) of the solvents enabling abrupt absorption of the Ag precursor and alcoholic solvents by the polymer.[44] The FE-SEM images shown in Fig. 3a and b reveal the SBS/$AgCF_3COO$ fiber before and after the reduction of the Ag precursor into AgNPs, respectively. After the reduction of $AgCF_3COO$ by $N_2H_4{\cdot}4H_2O$, AgNPs were uniformly generated and distributed within the fiber which is clearly seen from Fig. 3b. The interconnections of AgNPs designate good electrical contact between adjacent particles providing a contribution to the electrical conductivity, and also, preservation of the electrical properties under strain. The FE-SEM image shown in Fig. 3c illustrates the cross-sectional morphology of the microporous PDMS-coated fiber. A magnified view of the microporous PDMS structure is presented in the inset of Fig. 3c. The spatial distribution of the micropores was characterized through X-ray micro-CT as depicted in Fig. S1, ESI.† The pores having unequal pore sizes ranging from 43 μm to 148 μm were randomly distributed as seen from FE-SEM and micro-CT images. Due to the inclusion of micropores on PDMS, the elastic modulus of the dielectric film was also decreased as compared to solid PDMS. The elastic modulus as a function of pressure is depicted in detail in Fig. S2, ESI.† The average diameter of the pores was measured to be somewhat less than 95 μm, substantially smaller than previously reported work.[10] The porosity (ϕ) was calculated to be around 48.8% according to the following equation:

$$\phi = 1/(v_p/v_g + 1) \times 100\%,$$

where v_p and v_g represent the volume fraction of PDMS and glucose fillers, respectively. The porosity can be adjusted simply by adding different volume (weight) percents of glucose particles to the uncured PDMS elastomer. Three different glucose to polymer ratios, v_g/v_p, of 0.95, 1.3 and 1.7 corresponding to porosities of 48.8%, 56.5% and 63.0%, respectively, were coated on the surface of the conductive fibers. Lower porosities are difficult to achieve since the materials would contain trapped pockets of glucose which are hard to dissolve. Porosities of higher than 50% can ensure substantial change in the effective permittivity as a small pressure is sufficient to produce large deformation because of the reduced stiffness of the dielectric material. However, it is difficult to achieve porosity higher than 73.7% since the structure may collapse.[45] At a higher concentration of glucose particles corresponding to $v_g/v_p > 0.95$, the film structure suffered from unstable morphology since the composite hardly or could not flow along the fiber as the gravity is dominated by the surface tension. Refer to Fig. S3 (ESI†) for more details. In addition, a higher amount of glucose fillers such that $v_g/v_p > 0.95$ facilitated the enhancement of the sensitivity and elastic modulus of the dielectric, however, the sensitivity values calculated for each of the measurements were found to be inconsistent. The irregularity in the morphology results in an alteration in the sensitivity because of the inconsistency in the electrode separation, which is excluded from the present study. Therefore, in our sensor fabrication, a porosity of 48.8% was the trade-off between the sensitivity and the surface morphology. The details of the sensitivity and error deviation for different values of glucose to PDMS composition are presented in Table S1 and Fig. S4, ESI.†

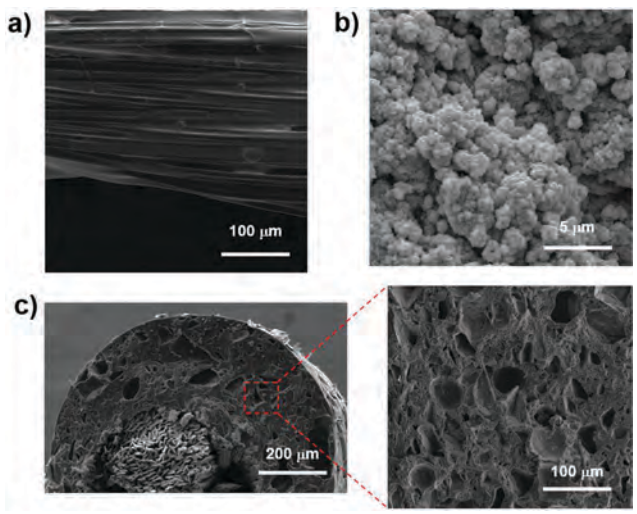

Fig. 3 (a) FE-SEM image of the SBS/$AgCF_3COO$ composite fiber before chemical reduction. (b) FE-SEM image of the fiber after chemical reduction of $AgCF_3COO$ by $N_2H_4{\cdot}4H_2O$. The AgNPs formed within the fiber provide good interconnection for electrical conductivity. (c) FE-SEM image of the cross-sectional view of the microporous PDMS-coated fiber. The inset of the figure shows the magnified view of the porous structure indicating random distribution of the micropores.

The conductivity of the fibers was significantly increased by a repeated number of absorption/reduction processes. Fig. 4a illustrates the resistance per unit length of conductive fiber against different cycles of absorption/reduction of the Ag precursor. After repeating the absorption/reduction process for up to eight cycles, the fiber showed an excellent electrical property with an ELR per unit length of 0.1431 Ω cm^{-1}, which is fairly excellent as compared to previously reported aluminum fibers (0.2 Ω cm^{-1})[14] and commercial conductive thread (1 Ω cm^{-1}). The theoretical value of conductivity of the fibers having diameter ~320 μm was calculated to be ~87 S cm^{-1}. Furthermore, to observe the stability, we measured the electrical property of the conductive fiber by a repeated number of folding tests. ELR values for every folding by an angle of 180° were measured and plotted as shown in Fig. 4b. For over 100 folding cycles, the ELR per unit length was slightly increased from 0.1431 Ω cm^{-1} to 0.1469 Ω cm^{-1} indicating almost no degradation of the conductivity.

Characterization of the sensor

To quantitatively evaluate the performance of the sensor, capacitance and force values were measured as a function of compression distance. A schematic illustration and the setup

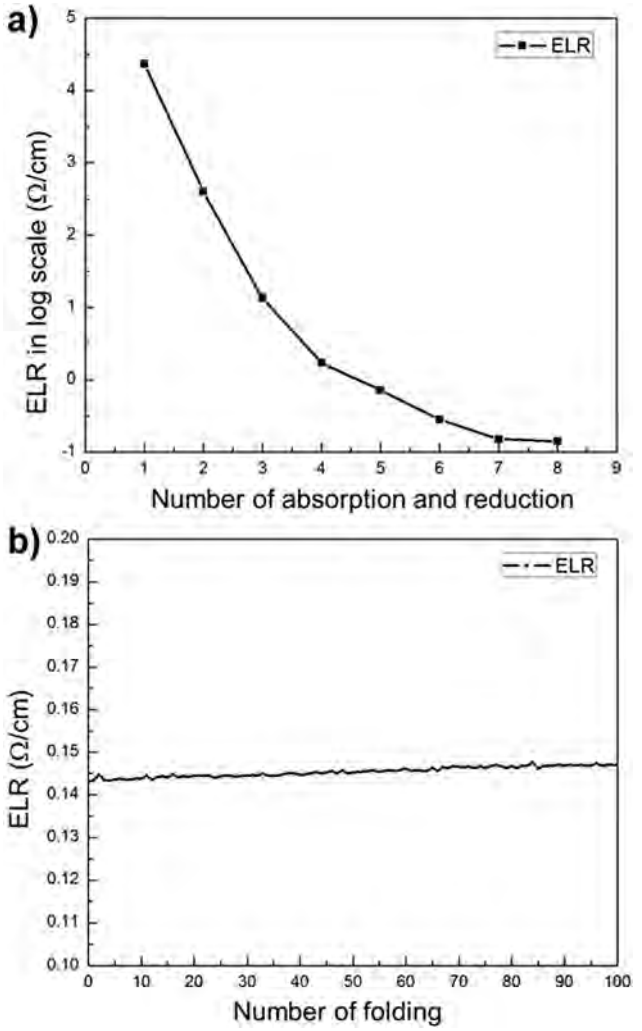

Fig. 4 (a) ELR per unit length (in log scale) with number of absorption/reduction cycles. (b) ELR per unit length of the conductive fiber with number of folds by 180°.

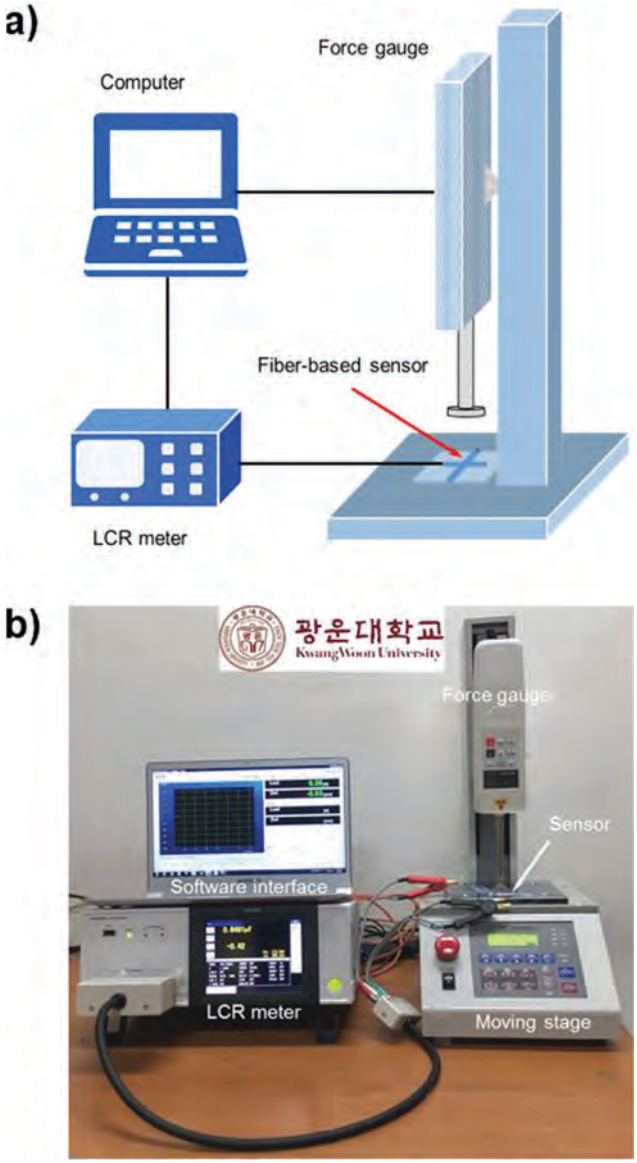

Fig. 5 (a) Schematic illustration of the experimental setup. (b) Experimental setup for the measurement of capacitance for applied pressures. Pressure was measured by applying a compressive force perpendicular to the area of an acrylic spacer attached to the moving stage's fixture.

for the measurement of capacitance corresponding to various pressures are shown in Fig. 5a and b, respectively.

For the hysteresis analysis, both types of features were loaded with a series of pressures from 0 kPa to 48.69 kPa and unloaded back. The hysteresis behavior of the sensors for a full span of the pressure cycle is shown in Fig. 6a. It was calculated from the normalized difference of the pressures between the forward and reverse paths. For the microporous PDMS-coated feature, the loading pressure of 48.69 kPa corresponded to the compression distance of 1.4 mm (60.86% strain), whereas, the same value of loading pressure corresponded to 1.12 mm (53.33% strain) for the solid PDMS-coated feature. The negligible value of hysteresis ($\sim$6.3%) calculated for the microporous PDMS-coated feature indicates that the sensor performance was almost perfectly reversible indicating the more resilient nature of microporous PDMS.

To evaluate the sensitivity of the sensor, normalized values of change in capacitance with pressure were measured as shown in Fig. 6b. The slope of the trace represents the sensitivity (S) of the pressure sensor which is typically related as

$$S = (\Delta C/C_0)/\Delta P,$$

where ΔP denotes the change in applied pressure, and ΔC and C_0 denote the relative change in capacitance and capacitance with no applied pressure, respectively. The sensor showed three different sensitivity characteristics within the textile pressure range (0–50 kPa). The pressure sensitivities of 0.278 kPa^{-1} for <2 kPa, 0.104 kPa^{-1} for 2–10 kPa, and 0.0186 kPa^{-1} for >15 kPa were obtained for the microporous PDMS-coated sensor, which are substantially higher than that of previously reported conductive fiber-based pressure sensors with solid elastomers.[5] A more generalized view of the sensitivity plot

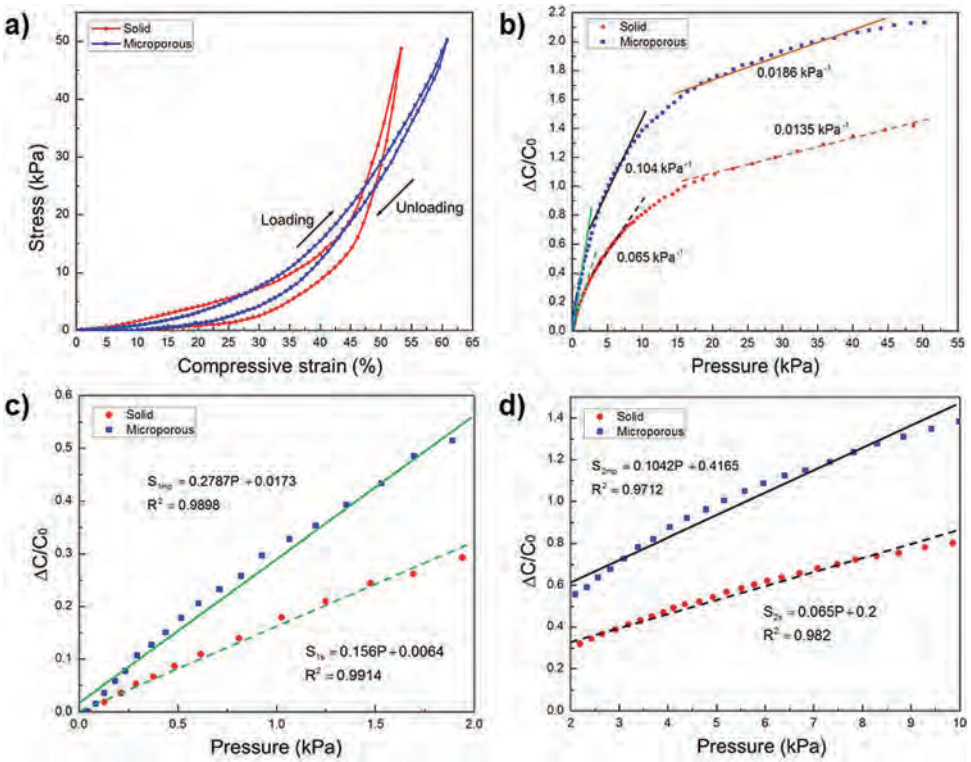

Fig. 6 (a) Stress–strain behavior of the sensor for the loading and unloading of various pressures. (b) Relative capacitance change with respect to progressively increasing pressures. The microporous PDMS-coated type sensor exhibited a much higher pressure sensitivity than the solid PDMS-coated type for the same coating thickness. (c) Relative change in capacitance in response to external pressures of <2 kPa. (d) Relative change in capacitance in response to external pressures of 2–10 kPa.

for <2 kPa pressure is shown in Fig. 6c. The high sensitivity value of 0.278 kPa^{-1} with linear fitting of *R*-square of 0.9898 was obtained in the low pressure region (<2 kPa). In this region, the sensitivity of the sensor is significantly enhanced by three key factors, *viz.* reduced distance between electrode fibers, increased contact area between electrode fibers and increased effective permittivity of the dielectric. Specifically, under an identical pressure level, microporous features can produce significant capacitance change as compared to solid features since the vacuum fraction of the micropores is large enough to produce substantial deformation. The vacuum fraction with $\varepsilon_a \approx 1$ is replaced by the neighbouring PDMS dielectric with $\varepsilon_p \approx 3$ contributing further enhancement in effective permittivity. Likewise, for the pressure range 2–10 kPa, the sensitivity was found to be 0.104 kPa^{-1} with *R*-square of 0.9712 as shown in Fig. 6d. The sensitivity at this pressure range was found to slightly decrease as compared to the sensitivity in the low pressure region. This characteristic presumably resulted from fairly increased elastic resistance of the dielectric since the pores were already almost fully closed. Furthermore, in the high pressure region (>15 kPa), the sensitivity of the microporous structure (~ 0.0186 kPa^{-1}) was found to be slightly higher than that of the solid structure (~ 0.0135 kPa^{-1}); see, Fig. S5, ESI.† In this pressure region, the contact area induces lower effective stress and the permittivity of the microporous dielectric also gets saturated resulting in almost similar characteristics to a solid structure. The lower limit of detection (LOD) of the proposed sensor was examined by placing a small coffee grain with a mass of ~ 4 mg corresponding to a pressure of ~ 38.82 Pa. While loading the pressure of 38.82 Pa, the sensor capacitance changed from 0.1045 pF to 0.1153 pF. This indicates the ultralight weight object detection capabilities of the proposed sensor. The sensor offered ultrahigh sensitivity to low pressures because of the increased effective permittivity and high compliance of the microporous structure. The sensitivity values for fiber-based capacitive pressure sensors for different pressure ranges are compared in Table 2. Relatively high sensitivity for the low pressure regime is desirable for detection of subtle pressure generated from the human body. The prime focus of our approach is on biocompatiblity, flexiblity, low cost and simple fabrication with high sensitivity.

The response and relaxation times for both types of features for pressure ranges <2 kPa and 2–10 kPa were measured as shown in Fig. 7a. For the loading and unloading of constant pressures of 1.35 kPa and 7.82 kPa for the duration of 5 s, both types of features exhibited dynamic response times in the millisecond range (~ 340 ms). In addition, the relaxation time measured for the microporous PDMS-coated feature was about two times faster (~ 0.5 s) than that of the solid one. The time-scaled version of the response time during the loading of 7.85 kPa and relaxation time for unloading are shown in Fig. 7b and c, respectively.

Table 2 Comparison of the sensitivities for various pressure ranges for fiber-based capacitive type pressure sensors

Electrode	Dielectric	Pressure ranges (kPa)	Sensitivities (kPa^{-1})	Ref.
AgNPs	Solid PDMS	0–2	0.21	5
Ag NWs	Solid PDMS	0–50	~0.0004	13
PEDOT:PSS	UV-adhesive	0–26	0.017	27
AgNPs	Microporous PDMS	0–2	0.278	This work

Although the response time could not be measured lower than 0.33 s because of the limitation of the LCR meter, the relaxation time for the microporous-coated feature was found to be faster than the solid PDMS-coated feature. This better relaxation time for the microporous dielectric resulted due to reduced viscoelastic effects to a certain extent. In the solid PDMS, the viscoelastic behavior of the material can induce poor response and relaxation times. However, in the case of the microporous PDMS-coated feature, the presence of the micropores allows larger deformable surfaces to reversibly and rapidly store and release the elastic energy imposed by external pressure.[17]

Furthermore, the reliability of the sensor was investigated by loading and unloading cycling tests using a minimum pressure of 38.82 Pa and a maximum pressure of 17.43 kPa. The reliability of the microporous PDMS-coated type sensor is shown in Fig. 7d. The variation in the capacitances ranged from 0.1052 pF to 0.1197 pF at 38.82 Pa and 0.2902 pF to 0.3086 pF at 17.43 kPa indicating almost no significant change in capacitance. For several consecutive runs (>10 000), almost no difference in capacitance for pressure applied confirms that the sensor output is highly reproducible. Since a good stability is always an indispensable aspect for practical and long-term applications, the stable response of the sensor for more than 10 000 cycling tests confirms its consistency for practical applications.

In order to demonstrate the applicability of the sensor, the performance was analysed through a capacitance readout circuit. A capacitance readout circuit comprising an operational amplifier and a full-wave rectifier module was designed to produce an output voltage proportional to the input capacitance change. The details of the circuit diagram and photographic image of the circuit board are shown in Fig. S6 and S7, respectively; see the ESI.† The circuit functions by detecting small variations in capacitance during pressure being applied and converting the respective capacitance variation into an output voltage. The sensor was weaved into Coban self-adherent wrap as shown in Fig. 8a and an external pressure was applied through gentle finger touch. For an input voltage of 600 mV, 300 kHz, the output voltage obtained for random finger tapping at the rate of ~2 Hz is shown in Fig. 8b. Similarly, Fig. 8c corresponds to the response of the sensor to gentle pressing/releasing (<10 kPa) for the duration of ~2 s and Fig. 8d is for loading and unloading of small acrylic cubes (2 mm × 2 mm × 2 mm) of ~9.4 mg. From the output response of the sensor it is clear that

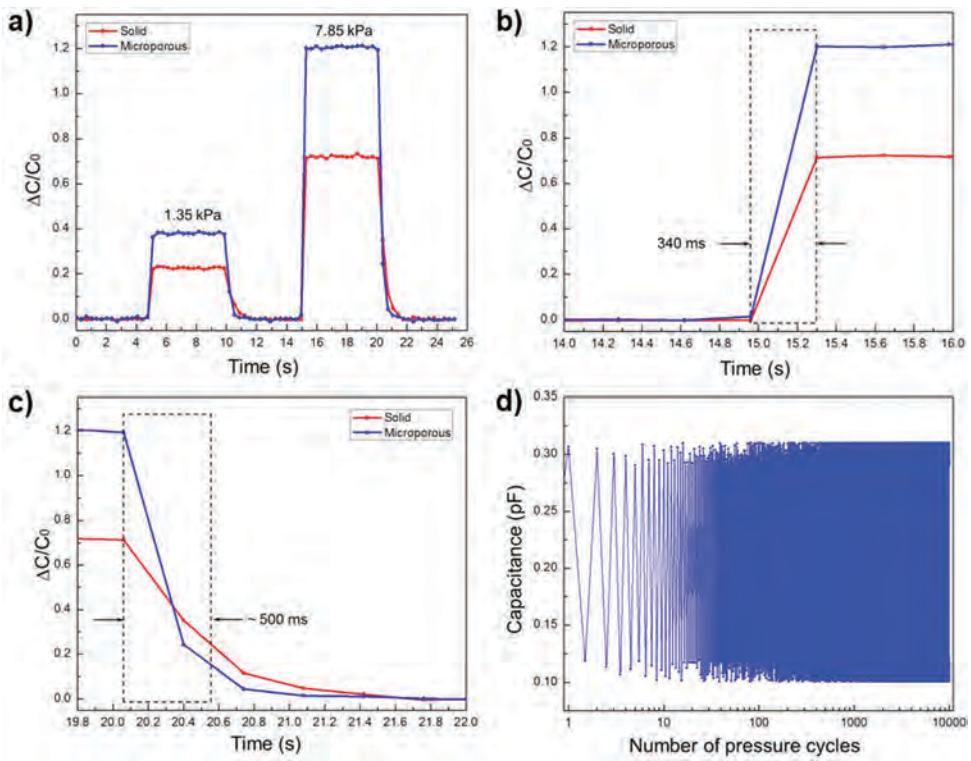

Fig. 7 (a) Dynamic response and relaxation times of the sensors for loading and unloading of two different pressures (1.35 kPa and 7.85 kPa). (b) Response time of the sensors for loading of 7.85 kPa pressure. The response time during the loading of pressure for both the features was observed to be almost the same. (c) Response time of the sensors for unloading of 7.85 kPa pressure. Relaxation time for the microporous PDMS-coated type was faster than that of the solid one. (d) Reliability test of the microporous PDMS-coated sensor measured for >10 000 cycles at a frequency of 1 Hz. No significant change in capacitance shows the stable response of the sensor for several consecutive runs.

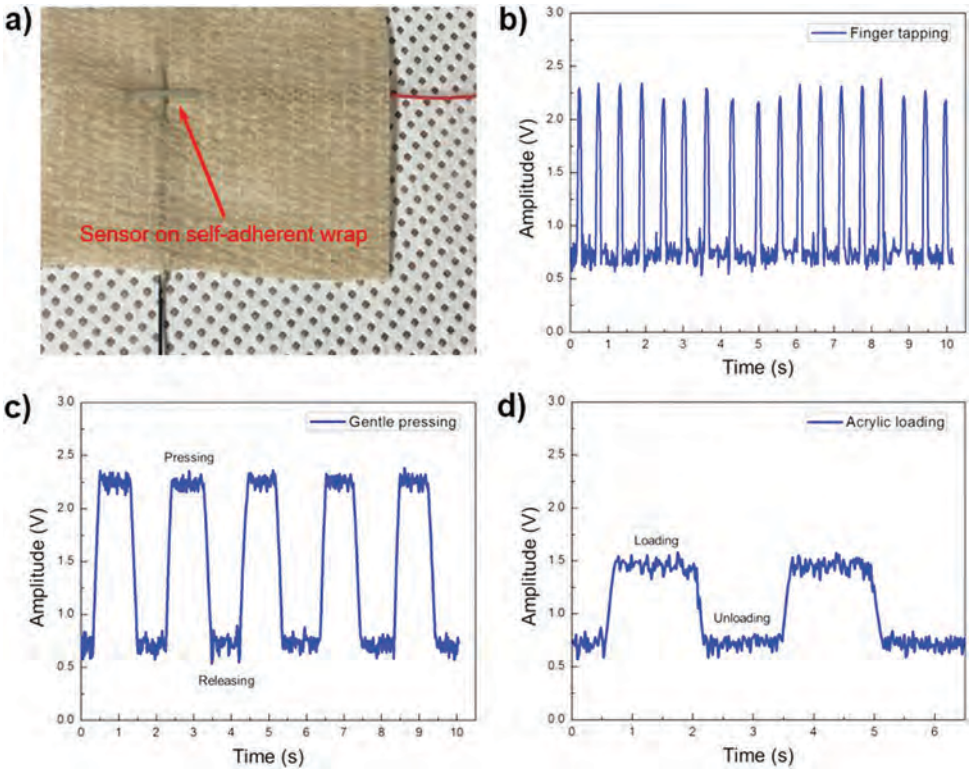

Fig. 8 (a) Photographic image of the sensor weaved into Coban self-adherent wrap. (b) Output of the circuit for random finger tapping of the sensor. (c) Response of the circuit for five consecutive gentle pressing and releasing (<10 kPa) cycles. The stable output and abrupt switching between voltage levels indicate an immediate response of the circuit. (d) Output of the capacitance detection circuit for the loading and unloading of an acrylic sheet (~9.4 mg) for a few seconds.

the sensor was able to precisely distinguish pressure loading through capacitance variation which in turn successfully transformed into corresponding output voltages. In addition, the output of the circuit retained steady voltage levels for the loading and unloading of pressure, and also, there was an abrupt switching between the corresponding voltage levels. Based on these characteristics, it confirms that our sensor has potential scope in the field of wearable applications such as object detection for e-skin, human–machine interface and health status monitoring systems. The wearable sensors with high sensitivity, low modulus, light weight, and high flexibility and stretchablity, which can conformally contact with human body organs and skin can provide new opportunities for personal health-care and human-activity monitoring. Ultrasensitive pressure sensors can measure subtle pressure such as pulse and arterial wave-form, which can provide important information about cardiac health status. Such kinds of sensors can also be imbedded into cloths or garments through a simple sewing and weaving method. A network of mechanically flexible sensors that can conformally contact to irregular surfaces can spatially map and quantify various external stimuli. As the sensitivity is high enough to detect small objects and gentle touches, it is also suitable for wearable keyboard applications. By using a comparator circuit with predefined threshold voltage, the change in voltage during pressing/releasing can be used to display the corresponding symbols.

Conclusions

In summary, we developed a flexible and wearable conductive fiber-based capacitive pressure sensor based on a microporous dielectric material. The conductive fibers were successfully prepared by coating SBS polymer on synthetic fibers followed by absorption/reduction of the Ag precursor into AgNPs. Likewise, the coating of a microporous dielectric elastomer was achieved through a mixture of PDMS elastomer and glucose particles. Due to the presence of the microporous structure within the dielectric layer, our sensor is highly deformable for small pressure levels. Moreover, the gradual closure of micropores for successive compression helps increase the effective permittivity, thereby enhancing the sensitivity. We achieved outstanding performance of the sensor with sensitivity of 0.278 kPa^{-1} for <2 kPa along with negligible hysteresis of 6.3%, dynamic range up to 50 kPa, and response time of ~340 ms, low detection limit of 38.82 Pa and an excellent stability and durability of >10 000 cycles. In addition, the applicability of the sensor performance was also analysed through a gentle finger touch (<10 kPa) by using a capacitance readout circuit. Based on excellent performance and the cost-effective fabrication process, we believe that our pressure sensor can provide new opportunities for next-generation advanced touch panels with a more human-friendly interface, non-invasive health monitoring systems, and artificial e-skin.

Conflicts of interest

There are no conflicts to declare.

Acknowledgements

This work was supported by the Technology Innovation Program (10065696) funded by the Ministry of Trade, Industry & Energy (MI, Korea), and the Bio & Medical Technology Development Program of the NRF funded by the Korean government, MSIP (2017M3A9F1031270). The authors would like to extend their gratitude to the Micro/Nano Devices and Packaging (MiNDaP) Laboratory group members of Kwangwoon University for their support and helpful discussions.

Notes and references

1 J. Kim, M. Lee, H. J. Shim, R. Ghaffari, H. R. Cho, D. Son, Y. H. Jung, M. Soh, C. Choi, S. Jung, K. Chu, D. Jeon, S. T. Lee, J. H. Kim, S. H. Choi, T. Hyeon and D. H. Kim, *Nat. Commun.*, 2014, **5**, 5747.
2 J. Park, Y. Lee, J. Hong, Y. Lee, M. Ha, Y. Jung, H. Kim, S. Y. Kim and H. Ko, *ACS Nano*, 2014, **8**, 12020.
3 C. Wang, D. Hwang, Z. Yu, K. Takei, J. Park, T. Chen, B. Ma and A. Javey, *Nat. Mater.*, 2013, **12**, 899.
4 E. Roh, B. U. Hwang, D. Kim, B. Y. Kim and N. E. Lee, *ACS Nano*, 2015, **9**, 6252.
5 J. Lee, H. Kwon, J. Seo, S. Shin, J. H. Koo, C. Pang, S. Son, J. H. Kim, Y. H. Jang, D. E. Kim and T. Lee, *Adv. Mater.*, 2015, **27**, 2433.
6 S. Jung, J. H. Kim, J. Kim, S. Choi, J. Lee, I. Park, T. Hyeon and D. H. Kim, *Adv. Mater.*, 2014, **26**, 4825.
7 S. Gong, W. Schwalb, Y. Wang, Y. Chen, Y. Tang, J. Si, B. Shirinzadeh and W. Cheng, *Nat. Commun.*, 2014, **5**, 3132.
8 C. Dagdeviren, Y. Su, P. Joe, R. Yona, Y. Liu, Y. S. Kim, Y. Huang and J. A. Rogers, *Nat. Commun.*, 2014, **5**, 4496.
9 Y. L. Tai and Z. G. Yang, *J. Mater. Chem. B*, 2015, **3**, 5436.
10 D. Kwon, T. I. Lee, J. Shim, S. Ryu, M. S. Kim, S. Kim, T. S. Kim and I. Park, *ACS Appl. Mater. Interfaces*, 2016, **8**, 16922.
11 C. M. Boutry, A. Nguyen, Q. O. Lawal, A. Chortos, S. R. Gangne and Z. Bao, *Adv. Mater.*, 2015, **27**, 6954.
12 L. Cai, L. Song, P. Luan, Q. Zhang, N. Zhang, Q. Gao, D. Zhao, X. Zhang, M. Tu, F. Yang, W. Zhou, Q. Fan, J. Luo, W. Zhou, P. M. Ajayan and S. Xie, *Sci. Rep.*, 2013, **3**, 3048.
13 B. Zhang, Z. Xiang, S. Zhu, Q. Hu, Y. Cao, J. Zhong, Q. Zhong, B. Wang, Y. Fang, B. Hu, J. Zhou and Z. Wang, *Nano Res.*, 2014, **7**, 1488.
14 H. M. Lee, S. Y. Choi, A. Jung and S. H. Kom, *Angew. Chem., Int. Ed.*, 2013, **52**, 7718.
15 S. Lee, S. Shin, S. Lee, J. Seo, J. Lee, S. Son, H. J. Cho, H. Algadi, S. A. Sayari, D. E. Kim and T. Lee, *Adv. Funct. Mater.*, 2015, **25**, 3114.
16 B. Y. Lee, J. Kim, H. Kim, C. Kim and S. D. Lee, *Sens. Actuators, A*, 2016, **240**, 103.
17 S. C. B. Mannsfeld, B. C.-K. Tee, R. M. Stoltenberg, C. V. H.-H. Chen, S. Barman, B. V. O. Muir, A. N. Sokolov, C. Reese and Z. Bao, *Nat. Mater.*, 2010, **9**, 859.
18 D. J. Lipomi, M. Vosgueritchian, B. C.-K. Tee, S. L. Hellstrom, J. A. Lee, C. H. Fox and Z. Bao, *Nat. Nanotechnol.*, 2011, **6**, 788.
19 J. Wang, J. Jiu, M. Nogi, T. Sugahara, S. Nagao, H. Koga, P. He and K. Suganuma, *Nanoscale*, 2015, **7**, 2926.
20 T. Yamada, Y. Hayamizu, Y. Yamamoto, Y. Yomogida, A. I. Najafabadi, D. N. Futaba and K. Hata, *Nat. Nanotechnol.*, 2011, **6**, 296.
21 C. Pang, G. Y. Lee, T. Kim, S. M. Kim, H. N. Kim, S. H. Ahn and K. Y. Suh, *Nat. Mater.*, 2012, **11**, 795.
22 T. Sharma, S. S. Je, B. Gill and J. X. J. Zhang, *Sens. Actuators, A*, 2012, **177**, 87.
23 C. T. Lee and Y. S. Chiu, *Appl. Phys. Lett.*, 2015, **106**, 073502.
24 M. Rothmaier, M. P. Luong and F. Clemens, *Sensors*, 2008, **8**, 4318.
25 M. Ramuz, B. C.-K. Tee, J. B.-H. Tok and Z. Bao, *Adv. Mater.*, 2012, **24**, 3223.
26 S. Kang, J. Lee, S. Lee, S. Kim, J.-K. Kim, H. Algadi, S. Al-Sayari, D.-E. Kim, D. Kim and T. Lee, *Adv. Electron. Mater.*, 2016, **2**, 1600536.
27 C. Lucarotti, C. M. Oddo, N. Vitiello and M. C. Carrozza, *Sensors*, 2013, **13**, 1435.
28 S. Takamatsu, T. Yamashita and T. Itoh, *Microsyst. Technol.*, 2016, **22**, 451.
29 L. Hu, M. Pasta, F. L. Mantia, L. Cui, S. Jeong, H. D. Deshazer, J. W. Choi, S. M. Han and Y. Cui, *Nano Lett.*, 2010, **10**, 708.
30 Y. Meng, Y. Zhao, C. Hu, H. Cheng, Y. Hu, Z. Zhang, G. Shi and L. Qu, *Adv. Mater.*, 2013, **25**, 2326.
31 Y. Atwa, N. Maheshwari and I. A. Goldthorpe, *J. Mater. Chem. C*, 2015, **3**, 3908.
32 X. Liu, X. Zhou, Y. Li and Z. Zheng, *Chem. – Asian J.*, 2012, **7**, 862.
33 F. Ochanda and W. E. Jones, *Langmuir*, 2005, **21**, 10791.
34 C. S. Boland, U. Khan, C. Backes, A. O'Neill, J. McCauley, S. Duane, R. Shanker, Y. Liu, I. Jurewicz, A. B. Dalton and J. N. Coleman, *ACS Nano*, 2014, **8**, 8819.
35 S. J. Pomfret, P. N. Adams, N. P. Comfort and A. P. Monkman, *Polymer*, 2000, **41**, 2265.
36 M. Z. Seyedin, J. M. Razal, P. C. Innins and G. G. Wallace, *Adv. Funct. Mater.*, 2014, **24**, 2957.
37 B. K. Little, Y. Li, V. Cammarata, R. Broughton and G. Mills, *ACS Appl. Mater. Interfaces*, 2011, **3**, 1965.
38 C. M. Boutry, A. Nguyen, Q. O. Lawal, A. Chortos, S. Rondeau-Gagne and Z. Bao, *Adv. Mater.*, 2015, **27**, 6954.
39 B. C.-K. Tee, A. Chortos, R. R. Dunn, G. Schwartz, E. Eason and Z. Bao, *Adv. Funct. Mater.*, 2014, **24**, 5427.
40 C. Pang, J. H. Koo, A. Nguyen, J. M. Caves, M.-G. Kim, A. Chortos, K. Kim, P. J. Wang, J. B.-H. Tok and Z. Bao, *Adv. Mater.*, 2015, **27**, 634.
41 S. Miller and Z. Bao, *J. Mater. Res.*, 2015, **30**, 3584.
42 J. Xu, M. J. Dapino, D. Gallego-Perez and D. Hansford, *Sens. Actuators, A*, 2009, **153**, 24.
43 F. Boulogne, M. A. Fardin, S. Lerouge, L. Pauchard and F. Giorgiutti-Dauphine, *Soft Matter*, 2013, **9**, 7787.
44 M. Park, J. Im, M. Shin, Y. Min, J. Park, H. Cho, S. Park, M.-B. Shim, S. Jeon, D.-Y. Chung, J. Bae, J. Park, U. Jeong and K. Kim, *Nat. Nanotechnol.*, 2012, **7**, 803.
45 A. Zhang, M. Chen, C. Du, H. Guo, H. Bai and L. Lil, *ACS Appl. Mater. Interfaces*, 2013, **5**, 10201.